Theoretical and Applied Fracture Mechanics 85 (2016) 125–133

Contents lists available at ScienceDirect

Theoretical and Applied Fracture Mechanics

journal homepage: www.elsevier.com/locate/tafmec

Influence of phase composition on the sliding wear of composites in the system $CaZrO_3$–MgO–ZrO_2 against ZrO_2 and steel

Abílio Silva [a,b,*], Fernando Booth [a,c], Liliana Garrido [c], Esteban Aglietti [c], Pilar Pena [a], Carmen Baudín [a]

[a] Instituto de Cerámica y Vidrio, ICV-CSIC, Kelsen 5, Madrid 28049, Spain
[b] Centre for Mechanical and Aerospace Science and Technologies (C-MAST-UBI), Universidade da Beira Interior, Rua Marquês d'Ávila e Bolama, 6201-001 Covilhã, Portugal
[c] CETMIC (Centro de Tecnología de Recursos Minerales y Cerámica, CIC-CONICET La Plata), Camino Centenario y 506, C.C.49 (B1897ZCA) M.B. Gonnet, Buenos Aires, Argentina

ARTICLE INFO

Article history:
Received 14 May 2016
Revised 31 July 2016
Accepted 19 August 2016
Available online 24 August 2016

Keywords:
$CaZrO_3$-MgO-ZrO_2
Wear
Fracture mechanism
SiO_2 effect
Dolomite

ABSTRACT

An attractive way to obtain low cost calcium zirconate ($CaZrO_3$) composites is mixing natural limestone or dolomite with zirconia. These $CaZrO_3$ based ceramic composites were often investigated as a promising high refractory for casting metal alloys, cements, thermal and environmental barrier coating.

In this study the sliding wear, fracture mechanism and friction properties of a $CaZrO_3$-MgO-ZrO_2 ceramic against ZrO_2 and steel counter bodies was carried out. Wear and fracture surface mechanisms, influence of its impurities and individual phases are discussed.

The composite presents a coefficient of friction higher in ceramic/metal than in ceramic/ceramic pair, but the specific wear it is significantly higher when tested with the ZrO_2 ball. The fracture surfaces present a dominant transgranular fracture when tested with steel and intergranular fracture against ZrO_2.

1. Introduction

Calcium zirconate ($CaZrO_3$) is a ceramic oxide of the perovskite family structure. Due to its high melting point (~2365 °C), high strength, high chemical inertness and excellent corrosion resistance against earth alkali oxides, and basic slags, in particular against KOH and mixtures of $NaVO_2$ and Na_2SO_4 environments, it has been proposed for high temperature applications. Calcium zirconate ($CaZrO_3$) is also an alternative refractory for casting several metals, in particular titanium and its alloys, because it shows similar chemical performance as CaO and it has the advantage of being inert to hydration, and having high temperature thermal stability and good handling strength [1–3].

Additionally, $CaZrO_3$ is the most stable compound in the system ZrO_2–CaO. Due to its thermal expansion behaviour ($\alpha \approx 10.4 \times 10^{-6}\,K^{-1}$), similar to that of yttria stabilised zirconia (YSZ) and its low thermal conductivity at high temperatures (2.0, 2.2 $W\,m^{-1}\,K^{-1}$ at 500 and 1500 K, respectively) it can be considered as an alternative to YSZ for thermal barrier coatings (TBC) [1,4–8]. TBC are used to increase the performance of turbine parts especially blades, in power production or energy conversion involving severe conditions of service: High temperature (up to 1400 °C), water vapour (≈10%), high pressure (up to 10 atm) steep thermal gradients, high gas velocities, and exposure to a corrosive environment, erosion and particles impact (sand, ash, salt) [8]. In addition to high temperature thermal stability (high melting point), low thermal conductivity and thermal expansion similar to that of the high temperature metallic superalloys used as substrates ($\approx 14 \times 10^{-6}\,K^{-1}$), $CaZrO_3$ has a relatively low density ($\approx 4.6\,g/cm^3$). Low densities contribute to the reduction of energetic consumption mainly in moving components while low thermal conductivities allow the increase of the operating temperatures with the consequent an increase in efficiency [7–10].

Calcium zirconate has to be synthesized because it is very rare in nature due to the high crystallization temperature of $CaZrO_3$ and the high activity of Si resulting in the formation of $ZrSiO_4$ instead of $CaZrO_3$. There are several ways to produce calcium zirconate, being the typical method the solid state reaction of equimolar CaO–ZrO_2 mixtures. The alternative method of using mixtures of zirconia with natural raw materials -limestone or dolomite- with consistent chemical composition is an attractive way for a low cost production of $CaZrO_3$-based materials. In this sense, dolomite based ceramics with heterogeneous microstructures have been investigated as a promising refractories for steel and cement industries [5,6,10–13].

In a previous work, the potential of reaction sintering of natural dolomite and zirconia to reach fine grained and dense $CaZrO_3$-MgO based composites to be used as structural materials was

* Corresponding author at: Centre for Mechanical and Aerospace Science and Technologies (C-MAST-UBI), Universidade da Beira Interior, Rua Marquês d'Ávila e Bolama, 6201-001 Covilhã, Portugal.
E-mail address: abilio@ubi.pt (A. Silva).

http://dx.doi.org/10.1016/j.tafmec.2016.08.017
0167-8442/

investigated [14]. Two natural dolomites were used as starting powders. One, DB, with low amounts of impurities (CaO + MgO = 97.4 wt.% and SiO_2 < 2 wt.%), and other DN, with medium amounts of impurities (CaO + MgO = 86.5 wt.% and SiO_2 = 10.2 wt.%). These natural dolomites were mixed, in proportion of 1:1 mol, with commercial ZrO_2 in order to obtain the final materials DBZ (low impurities content) and DNZ (medium impurities content).

Phase composition of the final materials (DBZ and DNZ) sintered at temperatures 1350–1450 °C was dramatically dependent of their impurities. The main differences are the amounts of $CaZrO_3$ (≈78 and 55 wt.%, for DBZ and DNZ, respectively), cubic ZrO_2 (≈2 and 15 wt.% for DBZ and DNZ, respectively) and the amounts of non-diffracting amorphous phases (≈4 and 10 wt.% for DBZ and DNZ, respectively), calculated by Rietveld analysis [14].

In the applications proposed for these $CaZrO_3$-MgO-ZrO_2 based ceramics -thermal and environmental barrier coatings and casting of titanium or steel alloys- the surface damage due to the surface interaction with other surfaces of particles is paramount for their performance. Sliding wear damage is a consequence, not only of the properties of the studied material but also of the work conditions, in particular, the characteristics of the sliding counterparts. Therefore, the wear characteristics of the $CaZrO_3$-MgO composite fabricated using the low silica dolomite (DBZ) in sliding contact with steel and ZrO_2 counter bodies was studied in a previous work [15]: Under severe wear conditions, with the same conditions of the present work, the coefficients of friction were higher for the ceramic/metal pairs (0.8–0.9) than for the ceramic/ceramic ones (0.6–0.7). However, the specific wear of the composite specimens was higher when sliding against ZrO_2 ($4.3–4.7 \times 10^{-4}$ mm^3 N^{-1} m^{-1}) than against steel ($0.7–0.9 \times 10^{-4}$ mm^3 N^{-1} m^{-1}) due to the different wear mechanisms occurring. When ZrO_2 was used as counterpart, fractured particles of the composite specimens formed dense layers that showed abrasion grooves and several cone cracks. Fracture and detachment of these layers led to further wear of the surfaces. When steel was used as counterpart, the formation of debris particles was accompanied by the transfer of significant amounts of steel to the composite surface. Cermet third body layers adhered to the specimen surfaces protected the ceramic leading to lower specific wear values. The capability of Fe to enter in solid solution in ZrO_2 as well as in MgO was identified as a determinant factor for adhesion of the third body when steel balls were used.

In this work, the wear behaviour of the $CaZrO_3$-MgO-ZrO_2 ceramic composite fabricated using the higher silica dolomite (DNZ) and sintered at 1450 °C [14] is studied in order to investigate the potential use of silica-rich compositions as raw materials. Main microstructural differences between the actual material (DNZ) and the previously studied one (DBZ, also sintered at 1450 °C) that, in principle, could affect the wear behaviour are the higher amount of c-ZrO_2, the larger grain sizes and the presence of localised regions of silica glasses [14]. In terms of crystalline phases, material DBZ can be practically considered as a two phase material $CaZrO_3$ and MgO, with minor (~5.7 wt.%) two crystalline phases of c-ZrO_2 and $Ca_3Mg(SiO_4)_2$ [14].

Room temperature pin-on disc experiments under un-lubricated conditions have been performed using two different tribo pairs: (i) DNZ ceramic against steel (ceramic/metal pair); (ii) DNZ ceramic against zirconia (ceramic/ceramic pair). Results are compared with those obtained for the low silica composite material, DBZ [15].

2. Experimental

Details of the processing procedure are reported elsewhere [14]. The starting material was a natural Argentinean dolomite (DN, 10.2 wt.% of SiO_2) and a commercial monoclinic zirconia, m-ZrO_2 (Saint Gobain - Zir Pro, China). The powders were mixed in proportion of 1:1 mol. Complete chemical analysis of DN, obtained by X-ray fluorescence technique (Philips, MagiX PW 2424, Netherlands), was reported elsewhere [14]. Main constituents of the burnt dolomite were (wt.%): CaO = 51.9, MgO = 34.6 and SiO_2 = 10.2. Main impurities (≈1 wt.%) were K_2O, Al_2O_3 and Fe_2O_3 and minor impurities (<0.2 wt.%) were Na_2O, P_2O_5 and TiO_2.

Mixing and milling was done by attrition milling in isopropyl alcohol with ZrO_2 balls during 4 h. Subsequently, the powders were dried at 60 °C during 24 h and unidirectional pressed at 20 MPa into cylinders with diameter of 10 mm and 8 mm of thickness and sintered at 1450 °C during 2 h. The result ceramic composite, namely DNZ present bulk density (g/cm^3) of 4.20 ± 0.03 and porosity (%) of 3.0 ± 0.5, where the purest composite (DBZ) has higher bulk density of 4.36 ± 0.04 g/cm^3 and 0% of porosity [14].

The surfaces to be subjected to sliding during the wear tests were diamond polished down to 3 μm, cleaned using ethanol and dried. The surface heights across five areas of 10 μm × 10 μm in the polished surfaces were recorded by atomic force microscope, AFM (Cervantes, Nanotec Electrónica, Spain) and the roughness of the surfaces was evaluated in terms of the Root Mean Square (RMS) values. Given values are the average of the five determinations and errors are the standard deviations. Additionally, different profiles along lines of 10–14 μm were recorded and the measured heights were correlated with the microstructural features observed by AFM. In order to understand the behavioural differences between the composite studied here, DNZ, and the one previously studied, DBZ, fully characterization of roughness of polished surfaces of this later was also performed.

Wear tests were performed on a pin-on-disk tribometer (tribotester UMT-3, CETR, Bruker, USA). The counter bodies were balls of 6.3 mm diameter made of stainless steel 440, ≈748 HV (MatWeb, www.matweb.com), and ZrO_2, ≈1300 HV (Hightech ceram Dr. Steinman, htc-YPSZ$_1$, Germany). All tests were performed at room temperature under a normal force (F) of 10 N at sliding speeds of 0.1 and 0.15 ms^{-1}. The track radius varied from 2 mm (0.1 ms^{-1}) to 5 mm (0.15 ms^{-1}), the frequency of contact was 7.96 Hz (0.1 ms^{-1}) and 4.77 Hz (0.15 ms^{-1}) and the total sliding distance (S) was equal to 500 m for all tests. During each test, the coefficient of friction (COF) was continuously recorded.

The microstructural characterization of the "as polished" surfaces as well as the wear tracks was analysed by scanning electron microscopy (SEM, Hitachi TM-1000, Japan) and field emission gun scanning electron microscopy (FE-SEM, Hitachi, S-4700, type I, Japan).

The volume of removed material was quantified using a contact profilometer (Bruker Dektak XT) by scanning the surface perpendicular to the wear track. First, four 2D profiles of sections of the wear track at 0, 90, 180 and 270° were done and the average of the hollow surfaces of the four profiles was calculated. The total wear volume after testing was then calculated by multiplying this average by the circumference of the wear track, in agreement with the standard ASTM G99. The specific wear rates K (mm^3 N^{-1} m^{-1}) were then calculated according to the following equation:

$$K = V/(F \cdot S) \quad (1)$$

where V is the volume of removed material (mm^3), F the normal load (N) and S the sliding distance (m).

3. Results

The complete microstructural characteristics of the studied material, DNZ, are reported elsewhere [14]. The main microstruc-

tural features are shown in Fig. 1b and c, and the microstructure of the high purity material DBZ is shown in Fig. 1a for comparison.

The DNZ material sintered at 1450 °C presented high density (4.20 ± 0.03 g/cm^3; 97 ± 1% R.D.) and the constituent phases were homogeneously distributed. According to the Rietveld analysis, major crystalline phases were $CaZrO_3$ (54.0 ± 0.9 wt.%), c-ZrO_2 ($Ca_{0.15}Zr_{0.85}O_{1.85}$, 17.5 ± 0.5 wt.%), MgO (16.2 ± 0.5 wt.%) and merwinite ($Ca_3Mg(SiO_4)_2$, 11.5 ± 1.2 wt.%). Ca_2SiO_4 was present in a very low amount (0.66 ± 0.3 wt.%) as minor phase [14].

Material DBZ was dense (≈100% T.D.) and homogeneous. Major crystalline phases were $CaZrO_3$ (75.4 ± 0.5 wt.%) and MgO (18.8 ± 0.4 wt.%); c-ZrO_2 ($Ca_{0.15}Zr_{0.85}O_{1.85}$, 2.2 ± 0.1 wt.%) and merwinite ($Ca_3Mg(SiO_4)_2$, 3.7 ± 0.3 wt.%) were present as minor phases [14].

Root Mean Square, RMS, values for DNZ and DBZ were 7 ± 3 and 5.7 ± 0.2 nm, respectively. In Fig. 2 characteristic distributions of surface heights across the 10 μm × 10 μm areas of the polished surfaces are shown. Distributions for different areas of DNZ (Fig. 2a) were extremely different and centred around a wide interval (10–60 nm). The distributions were fairly coincident for DBZ and centred between ≈5 and 35 nm (Fig. 2b).

Height profile lines for together with the corresponding AFM images of the studied areas are shown in Fig. 3.

As shown in Fig. 4, results for the evolution of the coefficient of friction (COF), for nominally identical sliding tests were fairly coincident. In the same way, differences between the specific wear for nominally identical tests were inside the variability limits of those obtained for one wear track.

Fig. 5 shows the evolution of the coefficient of friction (COF) with the sliding distance for the different testing conditions used. Results for the previously studied material are also plotted for comparison. The behaviours of both materials are similar for the tests performed with ZrO_2 balls (Fig. 5b and c). The COF attained constant values independent of the sliding rate after short running-in stages (≈70 m), which were slightly lower for the material studied here (0.65 and 0.7, for DNZ and DBZ, respectively).

The materials presented large differences when tested against steel balls. For DNZ tested at the lowest rate, the COF increased continuously (from 0.6 to 0.75) through the whole sliding distance while it reached a constant value (≈0.85) after a short distance (70 m) when the testing rate was 0.15 ms^{-1}. Conversely, highly variable COF that increased continuously (0.8–0.9) were recorded for DBZ specimens tested at both rates.

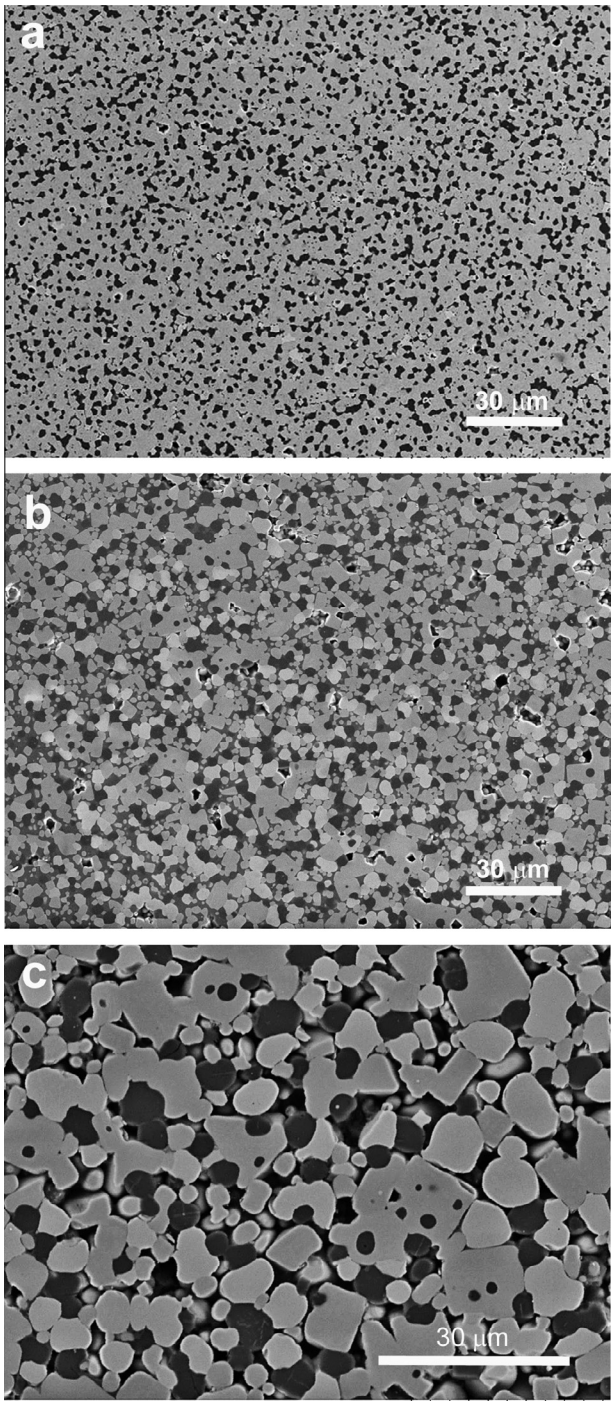

Fig. 1. Main microstructural features of the $CaZrO_3$-based composites. The black areas with shinny borders are pores. (a) DBZ. The matrix (dark gray) is $CaZrO_3$ and has a small amount of c-ZrO_2 particles and pores. The darkest particles correspond to MgO grains or SiO_2 glass. (b) DNZ. c-ZrO_2 (light gray) and $CaZrO_3$ (dark gray) particles are observed. The darkest particles correspond to MgO grains or SiO_2 glass. (c) DNZ. High magnification micrograph.

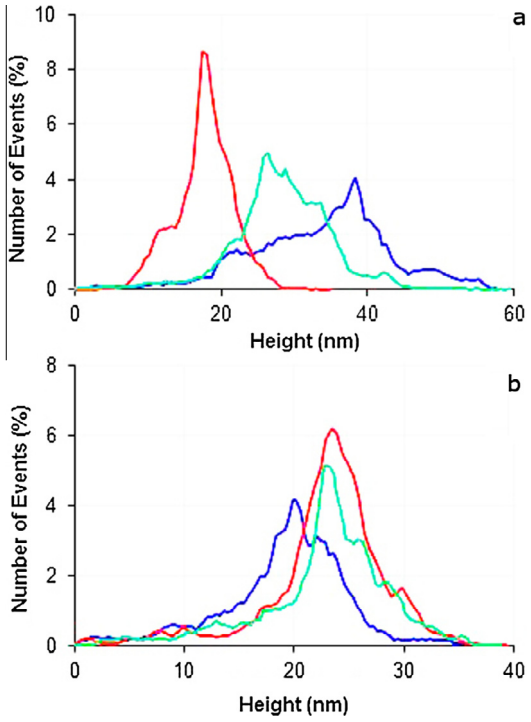

Fig. 2. Distributions of surface heights recorded by AFM in three 10 μm × 10 μm different areas of the polished surfaces. (a) DNZ. (b) DBZ.

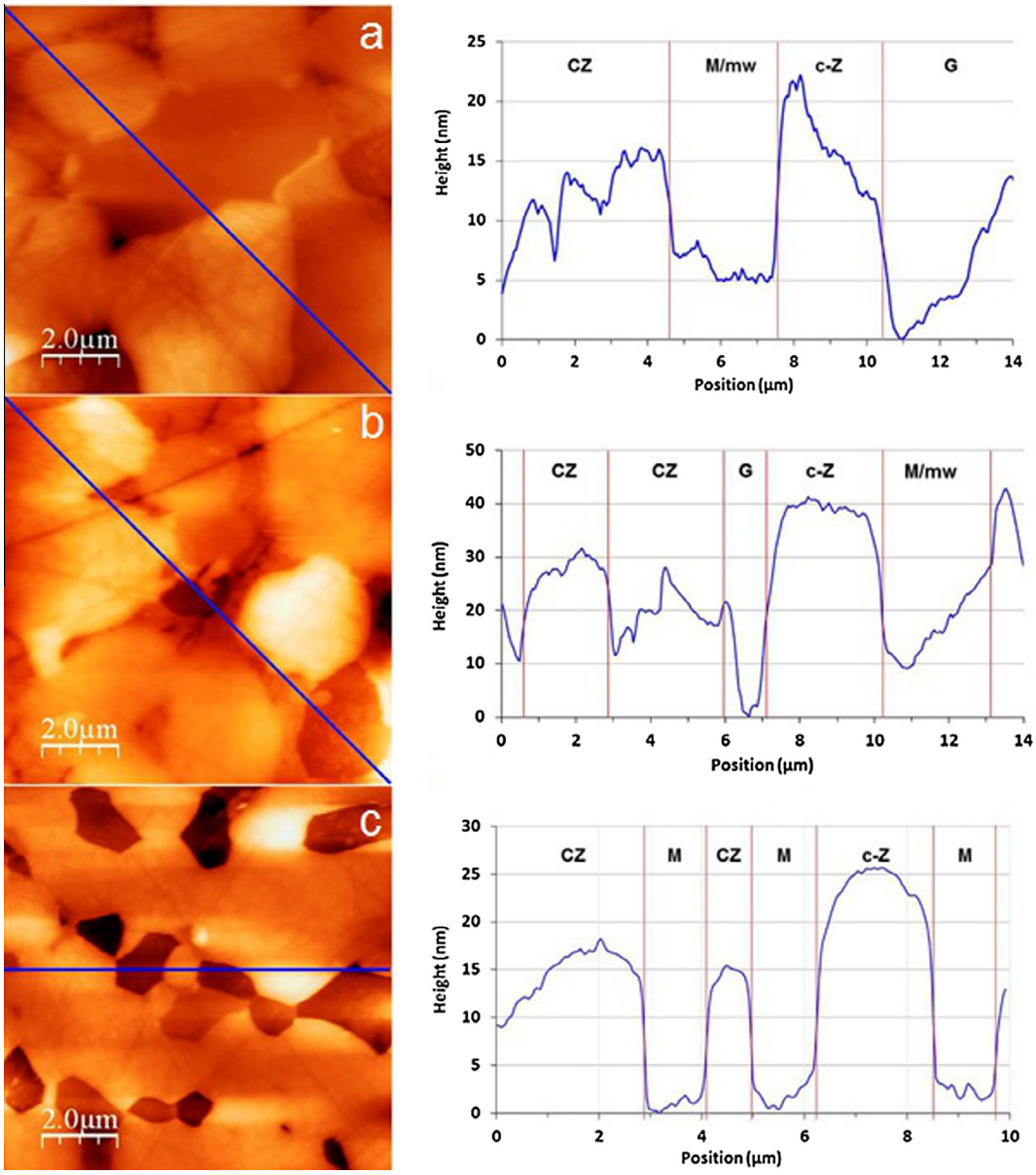

Fig. 3. AFM images of the polished surface of ceramic composites studied. CZ: $CaZrO_3$; c-Z: ZrO_2; M: MgO; mw: merwinite; G: glass. (a) and (b) Surface profile of DNZ. Analysis was done from top (x = 0 μm in the graph) to bottom (x = 14 μm in the graph). (c) Surface profile of DBZ. Analysis was done from left (x = 0 μm in the graph) to right (x = 10 μm in the graph).

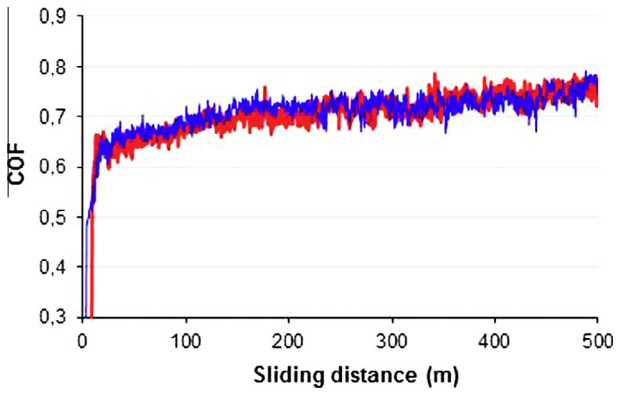

Fig. 4. Evolution of the coefficient of friction (COF) for nominally identical sliding tests of DNZ material performed at 0.1 ms^{-1} against steel ball.

Fig. 6 shows the specific wear (K) for the four experimental conditions used; results for DBZ are also plotted for comparison. For all combinations material composition- sliding rate, specific wears for tests performed using ZrO_2 (Fig. 6b) balls are significantly larger (≈10×) than when steel balls were used (Fig. 6a). For DNZ, values increase significantly with the sliding rate for both kinds of balls while they remained practically constant for DBZ. The highest wear rate is found for DNZ tested against ZrO_2 at the highest rate.

Fig. 7 shows the general aspect of the wear tracks formed in the tested specimens. All wear tracks present a regular aspect with well-defined edges and symmetrical arches. Track widths for the specimens tested using the steel balls (Fig. 7a) were about half of those formed when ZrO_2 balls were used (Fig. 7b).

The characteristic microstructural features of the wear tracks are summarised in Figs. 8 and 9. In order to understand the microstructural changes during the wear, the microstructure of the borders of the wear tracks was analysed separately from that

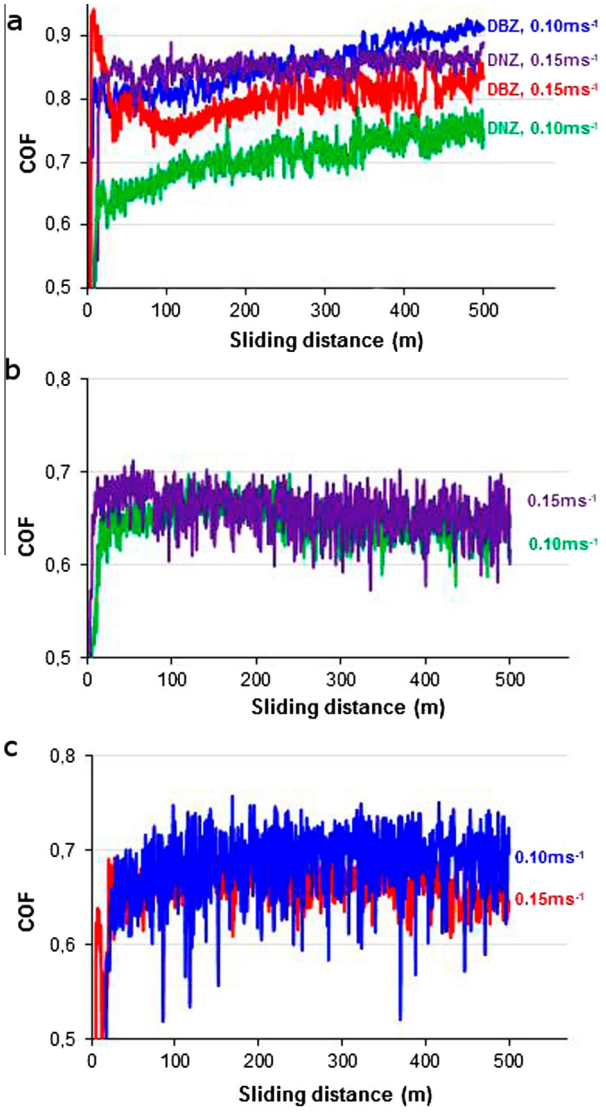

Fig. 5. Results of sliding tests for the studied material, DNZ together with those previously obtained for DBZ. Evolution of the coefficient of friction (COF) with the sliding distance for tests performed at the indicated rates. Average values for two different tests performed under nominally identical conditions are plotted. (a) DNZ and DBZ material tested with steel ball. (b) DNZ material tested with ZrO_2 ball. (c) DBZ material tested with ZrO_2 ball.

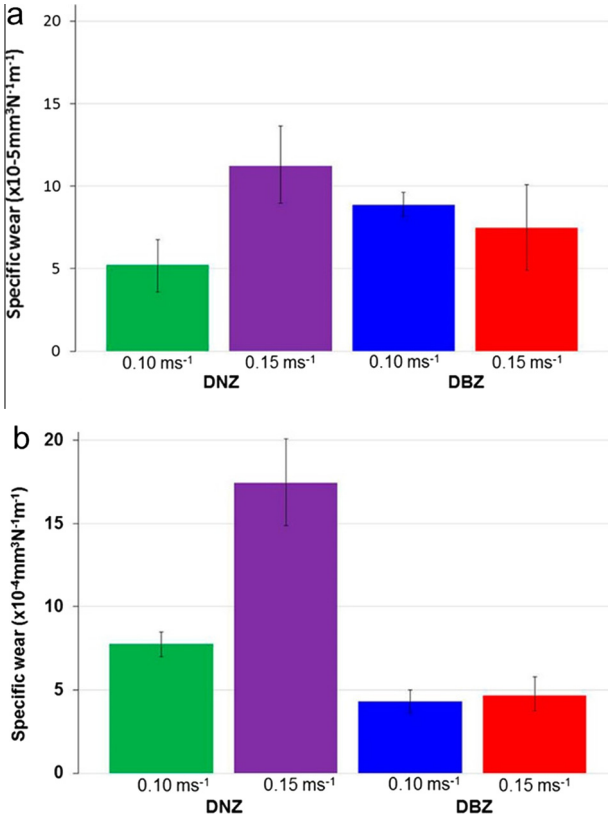

Fig. 6. Specific wear for the studied materials: DNZ and DBZ tested at indicated rates. (a) Specimens tested with steel balls. (b) Specimens tested with ZrO_2 balls.

of the central parts of the wear tracks. Microstructural modifications were similar for specimens tested using different sliding rates.

In the specimens tested using steel balls observed at low magnification (Fig. 8a and b) both regions of the tracks presented flat compacted surfaces and other zones with un-compacted debris particles. Higher magnification of the flat areas revealed heavily smeared surfaces with abrasion grooves (Fig. 8c and d). The main difference between the two track regions formed in these specimens were found in the un-compacted zones. Details of the border areas (Fig. 8e) revealed compact layers and debris particles and practically no original material was observed. In the central part of the tracks, large areas of the original material showing mainly transgranular fracture were observed (Fig. 8f).

Both regions of the tracks formed in the specimens tested using zirconia balls at observed at low magnification (Fig. 9a and b) presented flat compacted surfaces and zones with un-compacted debris particles. The compacted surfaces, which covered the major part of the tracks, presented cracks perpendicular to the sliding direction (Fig. 9c and d) and some abrasion grooves. In both regions, large zones of small (<1 μm) debris particles together with rounded particles were found (Fig. 9c and f).

Semi-quantitative EDX analyses of the different zones showed that the relative amounts of material components in the different zones of the wear tracks of the specimens tested using both kinds of balls (wt.%: SiO_2 = 6–9, MgO = 20–22, CaO = 17–24 and ZrO_2 = 55–59) were similar to those of the original material (wt.%: 4.69 of SiO_2, 15.90 of MgO, 23.84 of CaO and 55.57 of ZrO_2 [14]). However, in the specimens tested using steel, significant amounts of Fe (5–7 wt.%) and Cr (1–1.5 wt.%) were detected in the tracks, especially in the compacted areas, Fig. 8d and e.

4. Discussion

The size of the areas analysed to quantify roughness of the materials (10 μm × 10 μm) are sufficient to account for the general microstructure of material DBZ, which had much lower grain size ($CaZrO_3$ matrix between 1 and 3 μm [13]), than DNZ, in which the sizes of the particles in the $CaZrO_3$ matrix ranged to 3–10 μm (Fig. 1c). Thus, there were large differences between height distributions of different areas in material DNZ (Fig. 2a) while they were practically coincident in DBZ (Fig. 2b).

Roughness of the material studied here was much higher than that of DBZ, in spite of the same polishing procedure, which is explained by the different behaviours and amounts of the constituent phases during polishing. As it is well known, harder phases present higher resistance to polishing.

For DBZ, the identification of phases in the AFM images is straightforward from the aspect and frequency of the different particles. The most frequent and largest areas presenting medium height (10–20 nm) correspond to the $CaZrO_3$ matrix, the lesser frequent and smaller lowest areas (height ≈ 0 nm) would

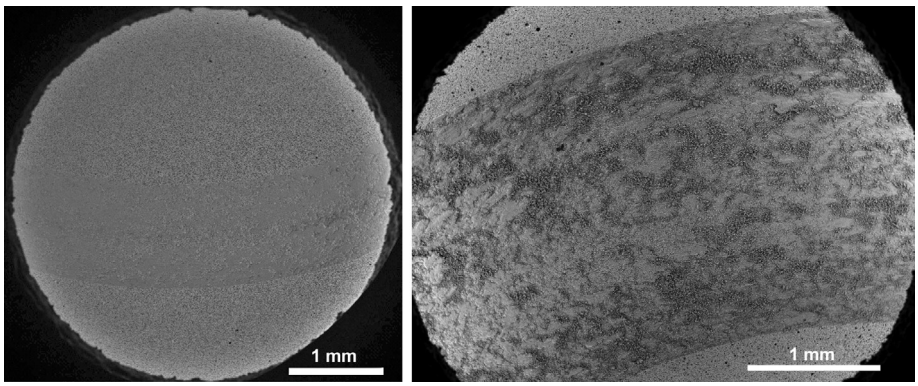

Fig. 7. General aspect of the wear tracks of the DNZ material. Characteristic low magnification SEM micrographs. (a) Specimen tested at 0.15 ms^{-1} with steel ball. (b) Specimen tested at 0.15 ms^{-1} with ZrO_2 ball.

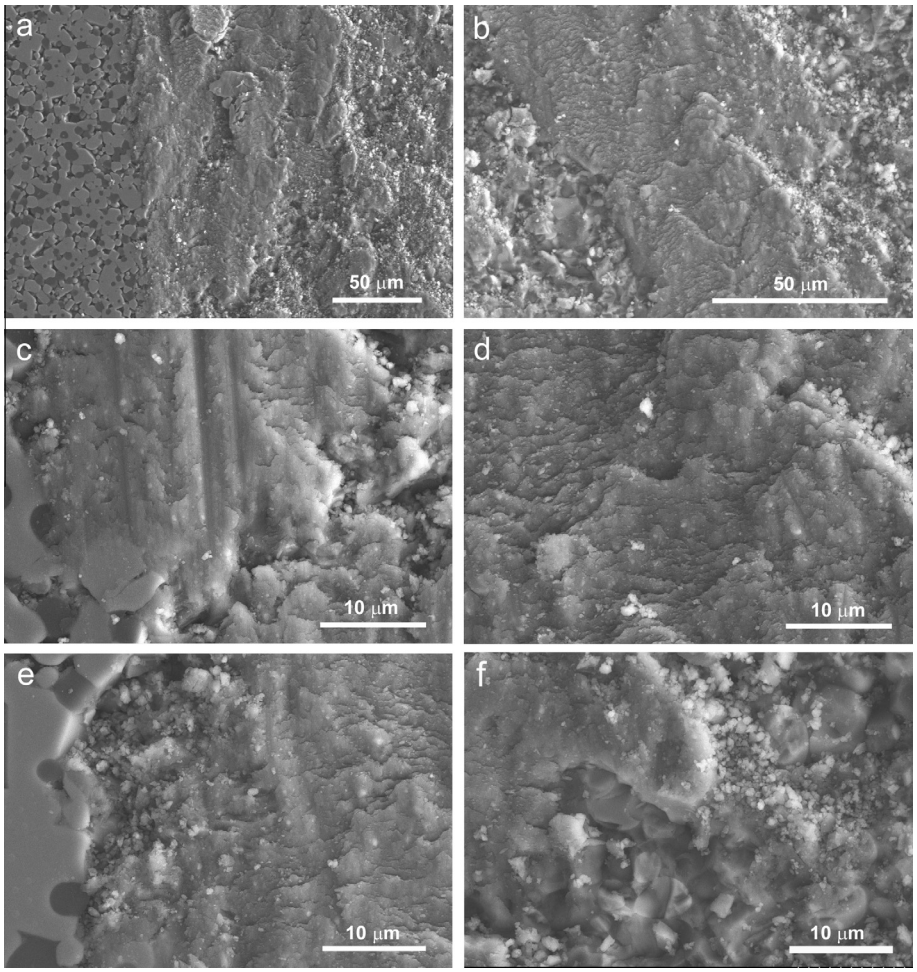

Fig. 8. Microstructural features found in the wear tracks in the test specimens of the studied material DNZ tested with steel balls. FE-SEM micrographs. Arrows show the sliding direction. (a), (b), (d), (e) and (f) At sliding rate of 0.1 ms^{-1}; (c) At sliding rate of 0.15 ms^{-1}. (a), (c) and (e) Border of the tracks (transition region). (b), (d) and (f) Central part of the tracks. (a) and (b) Low magnification micrographs. (c) Detail of (a) and (d) detail of (b) both showing a third body reacted with original grains. (e) Detail of (a) and (f) detail of (b) both showing fracture region and debris particles.

correspond to MgO particles (straight boundaries, Fig. 3c) while the least frequent and highest areas (25–40 nm) are c-ZrO_2. The different heights can be easily explained in terms of different hardness of the phases. MgO presents the lowest hardness (MgO: HV ≈ 9 GPa [16]), followed by $CaZrO_3$ (HV ≈ 11 GPa [17]), and c-ZrO_2 is the hardest one (CaO-c-ZrO_2: HV = 10–12 GPa, MgO-c-ZrO_2: HV = 12–14 GPa [18]).

The major phases in DNZ -$CaZrO_3$, MgO and c-ZrO_2- present the same relative heights as those above discussed, as shown in Fig. 3a and b. In this material, the c-ZrO_2 particles are larger and more frequent than in DBZ. As the hardness of merwinite (Mohs hardness = 6 [19]) is similar to that of magnesia (Mohs hardness = 5 [16]), it is not possible to differentiate these two phases in the AFM images. The 10 wt.% of glass present in this material

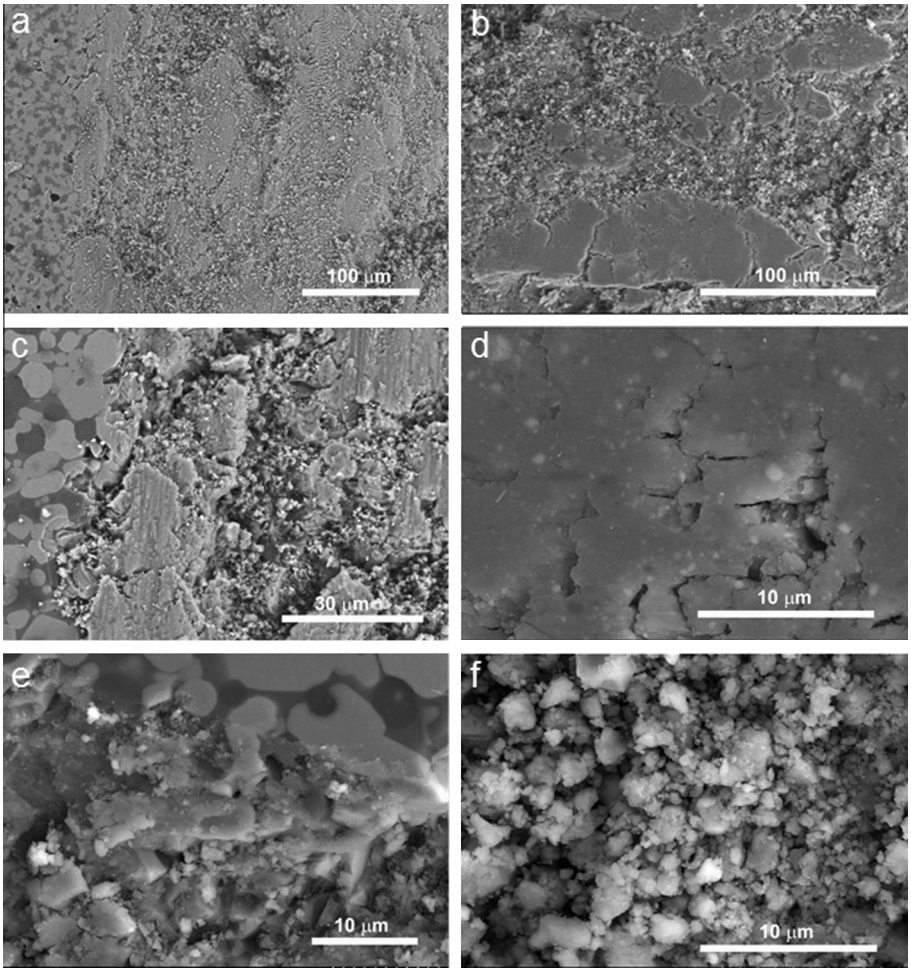

Fig. 9. Microstructural features found in the wear tracks in the test specimens of the studied material DNZ tested with ZrO_2 balls. FE-SEM micrographs. Sliding direction is from bottom to top of the micrographs. (a) and (c) At sliding rate of 0.15 ms^{-1}; (b), (d), (e) and (f) At sliding rate of 0.1 ms^{-1}. (a), (c) and (e) Transition border of the tracks (transition region). (b), (d) and (f) Central part of the tracks. (a) and (b) Low magnification micrographs. (c) Detail of (a) and (d) detail of (b), both showing a partial third body unstable reacted with original material. (e) Detail of (c) showing fracture surface with debris particles. (f) Detail of (b) showing fracture region rich on debris particles.

would correspond to the lowest height areas detected due to its low hardness (SiO_2 glass: HV ≈ 6 GPa [18]).

The slightly higher average roughness of DNZ (RMS = 7 ± 3 nm) as compared to that of DBZ (RMS = 5.7 ± 0.2) nm can be attributed to is due to the larger amount of c-ZrO_2 and glass.

From the analysis illustrated in Figs. 8 and 9, and the semi-quantitative chemical analysis of the different regions of the wear tracks, it is clear that the wear of the studied DNZ ceramic composite occurs through the formation of tribological layers, as previous reported by similar low silica content composition (DBZ [15]) and by others authors [20–26]. The formation of this tribofilm requires supply of building material in form of wear debris of suitable sizes that it is sufficiently well retained in the interface between the tested surface and that of the counterpart.

The values of the coefficient of friction (COF) obtained in this work after sliding 500 m against the counterpart of steel (0.7–0.9, Fig. 5a) are similar to those reported in the literature for un-lubricated (≈0.82) for 3Y-TZP (3 mol% yttria doped tetragonal zirconia polycrystal), using a rate of 1.0 ms^{-1} and a pressure of 1.0 MPa [26]; COF = 0.5–0.8 for zirconia-toughened alumina under higher load and one order of magnitude lower rate (20 N, 0.017 ms^{-1}) [27]; Also 3Y-TZP, tested under water lubrication (20 N, of 0.1 ms^{-1}) present COF = 0.6–0.86 [28].

In the same way, specific wear values (5.2–11.2 × 10^{-5} mm^3 N^{-1} m^{-1}, Fig. 6a) are in the range of those reported for Y_2O_3-stabilised ZrO_2 (3Y-TZP) sliding against steel under similar work conditions (10^{-5}–10^{-4} mm^3 N^{-1} m^{-1}) [27] and from 1.1 to 0.5 × 10^{-4} mm^3 N^{-1} m^{-1} for 3Y-TZP [28].

The specific wear and COF values obtained in this work for the specimens tested using ZrO_2 balls (Figs. 5b and 6b) are in the range of those reported for other structural ceramics tested using ceramic counter parts. In particular, similar values (specific wear between 10^{-3} and 10^{-4} mm^3 N^{-1} m^{-1}, COF = 0.55–0.65) were obtained for Y_2O_3-stabilised ZrO_2 materials tested using ZrO_2 balls and nominally the same experimental conditions as in this work [24].

The slightly larger surface roughness of material DNZ implies lower contact surface with the counterparts at the initial stages of the test. This would lead to a low COF though an accommodation distance until the asperities of the surface disappear. This accommodation distance is very short for the tests performed with ZrO_2 and for the tests run at the highest rate with steel balls (<50 m, Fig. 5a and b) while the COF continuously increases for tests performed at low velocity (0.10 ms^{-1}) with steel balls.

As occurred for the $CaZrO_3$-MgO composite previously studied (DBZ), specific wear values (≈10^{-5} mm^3 N^{-1} m^{-1}, Fig. 6a, and ≈10^{-4} mm^3 N^{-1} m^{-1}, Fig. 6b) obtained in this work correspond to severe wear of ceramics controlled by brittle fracture (specific wear >10^{-6} mm^3 N^{-1} m^{-1}) [28,29]. In fact, debris particles and detached grains are observed in the wear tracks of all specimens especially in the specimens tested with ZrO_2.

The differences between the track widths for the specimens tested with steel and with ZrO_2 balls (Fig. 7) should be function of the Young modulus and of hardness (H) of each phase of the material surface. From previous work [14] H_{DBZ} (7.8 GPa) is higher than H_{DNZ} (6.8 GPa). Based on the "rule of mixtures" the upper values of the Young modulus (E) of a composite can be calculated by the Voigt equation: -such as E_{DBZ} (≈234 GPa) is higher than E_{DNZ} (≈221 GPa). This way, the studied DNZ material, show higher track widths and higher volume of debris particles than the more purest DBZ material. Therefore, the higher values of DBZ ceramic surface for Young modulus, hardness and also the fracture strength (148 MPa and 108 MPa, for DBZ and DNZ, respectively [14]) contributes to the higher surface resistance of DBZ in comparison to DNZ.

Wear tracks are mainly constituted by compacted layers with grooves and no large cavities are observed in the tracks in specimens tested with steel, which would correspond to the mild wear stage [23,24]. The smeared layers observed in these specimens (Fig. 8a–e) are constituted by a cermet third body, formed as a result of the reaction between the counterpart of steel and the ceramic surface. This reaction is a combination of adhesion and ploughing processes. The adhesion mainly occurred because the chemical reaction between of the sample surface and the counterpart, when the ploughing was mainly due to the entrapment of debris particles [23]. Adhesive wear occurs mainly due to plastic deformation of the asperities and the increase of energy in these contact surfaces during the relative motion. This process also occurs due to strong adhesive forces between atoms, which indeed relates to chemical compatibility [25].

The worn surface tested with steel ball show a considerable amount of iron (Fe ≈ 14.5 wt.% and Cr ≈ 2.6 wt.%), much higher that its content in original composition (Fe ≈ 1.1 wt.%) [14]. Therefore, there is material transferred from the steel ball during the contact surfaces due the high temperature of friction and mutual chemical compatibility. State solid reaction between the steel ball (Fe) elements and the zirconia (system: ZrO_2-FeO-Fe) and periclase (system: $Mg_{1-x}Fe_xO$) were described in previous works [30,31], with a maximum of iron in solid solution of 5 mol% with ZrO_2 and could reach high values with MgO.

In central wear track, Fig. 8b, d and f, shows a stable third body and several regions with higher number of debris particles, Fig. 8f, where a partial fracture surface are visible result of a wear process more advanced. The stable third body, Fig. 8c and e, shows an irregular shape with severe abrasion grooves, mainly formed by layers with smeared surfaces, Fig. 8d. It seems that it are growing with the successive reaction between additional debris particles and the steel ball. This layer protect the surface of the original material, Fig. 8, and can be more resistant to delamination effect, thus, limiting the associated pull out [21]. These tribofilm worked as reducing frictional force between the contact surfaces because it increases the effect of hydrodynamic lubrication [21,24].

COF gradually increase significantly (≈0.75) with the sliding distance. At faster velocities (0.15 ms^{-1}) this effect is not so noticeable due to the faster formation of the protective cover. Nevertheless, it is observed also an increasing tendency and successive sudden variations in the value of the COF due to the cyclical destruction of parts of the cover. The volume of debris particles is lower because the reaction of adhesion between the ceramic/metal pair and when the third body pull out the transgranular fracture of the grains is predominant in the ceramic surface (Fig. 8f). However, specimens tested with ZrO_2 ball, shows round grains detached from the surface and large volume of debris particles are visible (Fig. 9f). Debris particles and original grains presenting intergranular fracture (Fig. 8e) due to the mechanical union between the ceramic/ceramic pair.

COF lowest value of the samples tested with ZrO_2 ball is due to the way of destruction of the ceramic surface. The DNZ material, present lower COF values (≈0.65) resulted of its larger roughness in comparison with DBZ material (≈0.70). Principally in the test performed with ZrO_2 ball, due the absence of adhesion reaction between the main phase of $CaZrO_3$ and the steel, the DNZ material with higher size grains and this impurities content are responsible for the higher value of removed material (Fig. 6). The thermal expansion mismatch between the several grains of the DNZ material is responsible for the intergranular facture [14,32].

Resulting from the wear against the counterpart of ZrO_2, Fig. 9a and b, shows a discontinuous and more unstable compacted cover, with high volume of debris particles. Fig. 9d confirms a discontinuous cover with many scratches in sliding direction, Fig. 9c, and a fracture surface with debris particles. The detail of the compacted cover, Fig. 9d, formed by mechanical pressure of the debris particles against the ceramic surface during the ZrO_2 ball sliding, shows a shape more flat that fill the voids and promotes a smoother tracking, with many deep fissures, Fig. 9b and d, mainly perpendicular to sliding direction as also reported by others authors [24,33].

5. Conclusion

During the sliding wear of DNZ material ($CaZrO_3$-MgO-ZrO_2-SiO_2) performed with ZrO_2 and steel balls it is clear that, under the current testing conditions, the coefficient of friction is higher in ceramic/metal pair than in ceramic/ceramic pair. Nevertheless the specific wear it is significantly higher and the depth of the wear trace against the counterpart of ZrO_2 is much deeper.

In ceramic/metal pair a stable cermet third body is formed as a result of the reaction between the counterpart of steel and the debris particles from fracture surface. This third body has irregular shape with severe abrasion grooves because is growing with successive reactions between additional debris particles and the steel ball, which correspond to the mild wear stage. This cover protects the surface of the original material reducing frictional force between the contact surfaces.

In ceramic/ceramic pair a discontinuous and unstable cover occurs because of the mechanical pressure of the debris particles against the ceramic surface and it is characterized by many deep fissures mainly perpendicular to sliding direction.

The impurity contents on DNZ material and their consequently higher sized grain, lower Young modulus, hardness and fracture strength, increases significantly the volume of removed material (specific wear) during the wear test, especially when tested with ZrO_2. In opposite with the solid solution cermet formed between the ceramic/steel pair, the cover in ceramic/ceramic pair is a result of the absence of reaction of the adhesion.

The fracture of the worn surface, of the DNZ studied material, tested with steel shows transgranular fracture of the grains. However, when the DNZ material is performed with ZrO_2, large areas of debris particles and discontinuous cover with abrasion grooves are observed. This cover shows many scratches in a sliding direction and intergranular fracture of the grains are predominant in the worn surface.

Both, DNZ and DBZ may be proposed for severe operating conditions, such as refractory for casting metal alloys, cements, thermal and environmental barrier coating, however the DNZ should be used on massive applications where the conditions of wear requirements are not so critical, such as ceramic/metal pair.

Acknowledgements

This work was performed in the frame of the CYTED network HOREF (312RT0453) and was supported by the Spanish Government under project MAT2013-48426-C2-1-R.

Abílio P. Silva acknowledges the support from the Portuguese national funding agency FCT - Fundação para a Ciência e a Tecnologia through the grant: SFRH/BSAB/105760/2014, the financial support of JECS Trust through mobility Contract 2015 97 and Instituto de Cerámica y Vidrio - CSIC.

References

[1] S. Schafföner, C.G. Aneziris, H. Berek, J. Hubálková, A. Priese, Fused calcium zirconate for refractory applications, J. Eur. Ceram. Soc. 33 (15–16) (2013) 3411–3418.
[2] M.G. Kim, S.K. Kim, Y.J. Kim, Effect of mold material and binder on metal-mold interfacial reaction for investment castings of titanium alloys, Mater. Trans. JIM 43 (4) (2002) 745–750.
[3] C. Yuan, X. Cheng, P.A. Withey, Investigation into the use of $CaZrO_3$ as a facecoat material in the investment casting of TiAl alloys, Mater. Chem. Phys. 155 (2015) 205–210.
[4] J.L. Rodríguez, M.A. Rodríguez, S. de Aza, P. Pena, Reaction sintering of zircon-dolomite mixtures, J. Eur. Ceram. Soc. 21 (3) (2001) 343–354.
[5] J.L. Rodriguez, C. Baudín, P. Pena, Relationships between phase constitution and mechanical behaviour in MgO-$CaZrO_3$-calcium silicate materials, J. Eur. Ceram. Soc. 24 (4) (2004) 669–679.
[6] S. Serena, M.A. Sainz, A. Caballero, The system Clinker-MgO-$CaZrO_3$ and its application to the corrosion behavior of $CaZrO_3$/MgO refractory matrix by clinker, J. Eur. Ceram. Soc. 29 (11) (2009) 2199–2209.
[7] C. Cano, M.I. Osendi, M. Belmonte, P. Miranzo, Effect of the type of flame on the microstructure of $CaZrO_3$ combustion flame sprayed coatings, Surf. Coat. Technol. 201 (2006) 3307–3313.
[8] D.R. Clarke, M. Oechsner, N.P. Padture, Thermal-barrier coatings for more efficient gas-turbine engines, Mater. Res. Bull. 37 (2012) 891–898.
[9] N.P. Padture, M. Gell, E.H. Jordan, Thermal barrier coatings for gas-turbine engine applications, Science 296 (2002) 280–284.
[10] M. Belmonte, Advanced ceramic materials for high temperature applications, Adv. Eng. Mater. 8 (8) (2006) 693–703.
[11] J. Szczerba, Z. Pedzich, The effect of natural dolomite admixtures on calcium zirconate-periclase materials microstructure evolution, Ceram. Int. 36 (2) (2010) 535–547.
[12] J.L. Rodríguez, P. Pena, Obtención de materiales de magnesia - circonato cálcico - silicato dicálcico por sinterización reactiva de mezclas de dolomita - circón. Estudio del procesamiento, Bol Soc Esp Ceram V 40 (6) (2001) 461–469.
[13] E.A. Rodríguez, G.A. Castillo, T.K. Dasa, R. Puente-Ornelas, Y. González, A.M. Arato, J.A. Aguilar-Martínez, $MgAl_2O_4$ spinel as an effective ceramic bonding in a MgO-$CaZrO_3$ refractory, J. Eur. Ceram. Soc. 33 (13–14) (2013) 2767–2774.
[14] F. Booth, L. Garrido, E. Aglietti, A. Silva, P. Pena, C. Baudín, $CaZrO_3$–MgO structural ceramics obtained by reaction sintering of dolomite-zirconia mixtures, J. Eur. Ceram. Soc. 36 (2016) 2611–2626.
[15] A. Silva, F. Booth, L. Garrido, E. Aglietti, P. Pena, C. Baudín, Sliding wear of CaZrO3-MgO composites against ZrO2 and steel, J. Eur. Ceram. Soc. (in press) http://dx.doi.org/10.1016/j.jeurceramsoc.2016.07.029.
[16] G. Feng, W.D. Nix, Indentation size effect in MgO, Scripta Mater. 51 (2004) 599–603.
[17] D.W. Richerson, Modern Ceramic Engineering, Properties, Processing and Use in Design, 2nd ed. rev. and expanded., Publ. Marcel Dekker, Inc., New York, 1992, p. 150 (Chapter 4).
[18] T.I. Hou, W.M. Kriven, Mechanical properties and microstructure of Ca_2SiO_4–$CaZrO_3$ composites, J. Am. Ceram. Soc. 77 (1) (1994) 65–72.
[19] J.L. Rodríguez, S. De Aza, P. Pena, Effect of agglomerate and grain size on the reaction sintering of zircon–dolomite mixtures, Brit. Ceram. Trans. 100 (4) (2001) 181–191.
[20] P.C. Verma, L. Menapace, A. Bonfanti, R. Ciudin, S. Gialanella, G. Straffelini, Braking pad-disc system: wear mechanisms and formation wear fragments, Wear 322–323 (2015) 251–258.
[21] C. Baudín, A. Tricoteaux, H. Joire, Improved resistance of alumina to mild wear by aluminium titanate additions, J. Eur. Ceram. Soc. 34 (2014) 69–80.
[22] O. Borrero-López, A.L. Ortiz, A.D. Gledhill, F. Guiberteau, T. Mrozc, L.M. Goldmanc, N.P. Padture, Microstructural effects on the sliding wear of transparent magnesium-aluminate spinel, J. Eur. Ceram. Soc. 32 (2012) 3143–3149.
[23] M. Hua, X. Wei, J. Li, Friction and wear behavior of SUS 304 austenitic stainless steel against Al_2O_3 ceramic ball under relative high load, Wear 265 (2008) 799–810.
[24] M.S. Suh, Y.H. Chae, S.S. Kim, Friction and wear behavior of structural ceramics sliding against zirconia, Wear 264 (2008) 800–806.
[25] C.X. Li, J. Xia, H. Dong, Sliding wear of TiAl intermetallics against steel and ceramics of Al_2O_3, Si_3N_4 and WC/Co, Wear 261 (2006) 693–701.
[26] H. Liu, Q. Xue, Wear mechanisms of zirconia/steel reciprocating sliding couple under water lubrication, Wear 201 (1996) 51–57.
[27] K. Kameo, K. Friedrich, J.F. Bartolomé, M. Díaz, S. López-Esteban, J.S. Moya, Sliding wear of ceramics and cermets against steel, J. Eur. Ceram. Soc. 23 (2003) 2867–2877.
[28] F. Kern, P. Palmero, F.G. Marro, A. Mestra, Processing of alumina-zirconia composites by surface modification route with enhanced hardness and wear resistance, Ceram. Int. 41 (2015) 889–898.
[29] K. Kato, K. Adachi, Wear of advanced ceramics, Wear 253 (2002) 1097–1104.
[30] O. Fabrichnaya, D. Pavlyuchkov, Assessment of experimental data and thermodynamic modeling in the Zr-Fe-O System, Metall. Mater. Trans. A 47 (2016) 152–159.
[31] I.H. Jung, S. Decterov, A.D. Pelton, Thermodynamic Modeling of the Fe-Mg-O system, J. Phys. Chem. Solids 65 (2004) 1683–1695.
[32] A. Obregón, J.L. Rodríguez-Galicia, J. López-Cuevas, P. Pena, C. Baudín, MgO–$CaZrO_3$-based refractories for cement kilns, J. Eur. Ceram. Soc. 31 (2011) 61–74.
[33] A. Amanov, J.H. Kim, Y.S. Pyun, T. Hirayama, M. Hino, Wear mechanisms of silicon carbide subjected to ultrasonic nanocrystalline surface modification technique, Wear 332–333 (2015) 891–899.